

Air Force Institute of Technology

**AFIT Scholar**

---

Faculty Publications

---

6-28-2023

## Intrinsic Point Defects (Vacancies and Antisites) in CdGeP<sub>2</sub> Crystals

Timothy D. Gustafson  
*Air Force Institute of Technology*

Nancy C. Giles  
*Air Force Institute of Technology*

Peter G. Schunemann  
*BAE Systems*

Kevin T. Zawilski  
*BAE Systems*

Kent L. Averett  
*Air Force Research Laboratory*

*See next page for additional authors*

Follow this and additional works at: <https://scholar.afit.edu/facpub>



Part of the [Atomic, Molecular and Optical Physics Commons](#), and the [Semiconductor and Optical Materials Commons](#)

---

### Recommended Citation

Gustafson, T. D., Giles, N. C., Schunemann, P. G., Zawilski, K. T., Averett, K. L., Slagle, J. E., & Halliburton, L. E. (2023). Intrinsic point defects (vacancies and antisites) in CdGeP<sub>2</sub> crystals. *Journal of Applied Physics*, 133(24), 245703. <https://doi.org/10.1063/5.0156144>

This Article is brought to you for free and open access by AFIT Scholar. It has been accepted for inclusion in Faculty Publications by an authorized administrator of AFIT Scholar. For more information, please contact [AFIT.ENWL.Repository@us.af.mil](mailto:AFIT.ENWL.Repository@us.af.mil).

---

**Authors**

Timothy D. Gustafson, Nancy C. Giles, Peter G. Schunemann, Kevin T. Zawilski, Kent L. Averett, Jonathan E. Slagle, and Larry E. Halliburton

RESEARCH ARTICLE | JUNE 28 2023

# Intrinsic point defects (vacancies and antisites) in CdGeP<sub>2</sub> crystals

T. D. Gustafson ; N. C. Giles ; P. G. Schunemann ; K. T. Zawilski ; K. L. Averett ; J. E. Slagle ; L. E. Halliburton 



*Journal of Applied Physics* 133, 245703 (2023)

<https://doi.org/10.1063/5.0156144>



View Online



Export Citation

CrossMark

## AIP Advances

Why Publish With Us?

-  **25 DAYS**  
average time to 1st decision
-  **740+ DOWNLOADS**  
average per article
-  **INCLUSIVE**  
scope

[Learn More](#)

# Intrinsic point defects (vacancies and antisites) in CdGeP<sub>2</sub> crystals

Cite as: J. Appl. Phys. 133, 245703 (2023); doi: 10.1063/5.0156144

Submitted: 26 April 2023 · Accepted: 5 June 2023 ·

Published Online: 28 June 2023



T. D. Gustafson,<sup>1,a)</sup> N. C. Giles,<sup>1</sup> P. G. Schunemann,<sup>2</sup> K. T. Zawilski,<sup>2</sup> K. L. Averett,<sup>3</sup> J. E. Slagle,<sup>3</sup> and L. E. Halliburton<sup>4,5,a)</sup>

## AFFILIATIONS

<sup>1</sup>Department of Engineering Physics, Air Force Institute of Technology, Wright-Patterson Air Force Base, Ohio 45433, USA

<sup>2</sup>BAE Systems, Nashua, New Hampshire 03061, USA

<sup>3</sup>Air Force Research Laboratory, Materials and Manufacturing Directorate, Wright-Patterson Air Force Base, Ohio 45433, USA

<sup>4</sup>Azimuth Corporation, 2970 Presidential Drive, Suite 200, Beaver Creek, Ohio 45324, USA

<sup>5</sup>Department of Physics and Astronomy, West Virginia University, Morgantown, West Virginia 26506, USA

<sup>a)</sup>Authors to whom correspondence should be addressed: [Larry.Halliburton@mail.wvu.edu](mailto:Larry.Halliburton@mail.wvu.edu) and [Timothy.Gustafson@protonmail.com](mailto:Timothy.Gustafson@protonmail.com)

## ABSTRACT

Cadmium germanium diphosphide (CdGeP<sub>2</sub>) crystals, with versatile terahertz-generating properties, belong to the chalcopyrite family of nonlinear optical materials. Other widely investigated members of this family are ZnGeP<sub>2</sub> and CdSiP<sub>2</sub>. The room-temperature absorption edge of CdGeP<sub>2</sub> is near 1.72 eV (720 nm). Cadmium vacancies, phosphorous vacancies, and germanium-on-cadmium antisites are present in as-grown CdGeP<sub>2</sub> crystals. These unintentional intrinsic point defects are best studied below room temperature with electron paramagnetic resonance (EPR) and optical absorption. Prior to exposure to light, the defects are in charge states that have no unpaired spins. Illuminating a CdGeP<sub>2</sub> crystal with 700 or 850 nm light while being held below 120 K produces singly ionized acceptors (V<sub>Cd</sub><sup>-</sup>) and singly ionized donors (Ge<sub>Cd</sub><sup>+</sup>), as electrons move from V<sub>Cd</sub><sup>2-</sup> vacancies to Ge<sub>Cd</sub><sup>2+</sup> antisites. These defects become thermally unstable and return to their doubly ionized charge states in the 150–190 K range. In contrast, neutral phosphorous vacancies (V<sub>P</sub><sup>0</sup>) are only produced with near-band-edge light when the crystal is held near or below 18 K. The V<sub>P</sub><sup>0</sup> donors are unstable at these lower temperatures and return to the singly ionized V<sub>P</sub><sup>+</sup> charge state when the light is removed. Spin-Hamiltonian parameters for the V<sub>Cd</sub><sup>-</sup> acceptors and V<sub>P</sub><sup>0</sup> donors are extracted from the angular dependence of their EPR spectra. Exposure at low-temperature to near-band-edge light also introduces broad optical absorption bands peaking near 756 and 1050 nm. A consistent picture of intrinsic defects in II-IV-P<sub>2</sub> chalcopyrites emerges when the present CdGeP<sub>2</sub> results are combined with earlier results from ZnGeP<sub>2</sub>, ZnSiP<sub>2</sub>, and CdSiP<sub>2</sub>.

© 2023 Author(s). All article content, except where otherwise noted, is licensed under a Creative Commons Attribution (CC BY) license (<http://creativecommons.org/licenses/by/4.0/>). <https://doi.org/10.1063/5.0156144>

## I. INTRODUCTION

Cadmium germanium diphosphide (CdGeP<sub>2</sub> or simply CGP) is a tetrahedrally bonded semiconductor analogous to GaP. The CdGeP<sub>2</sub> crystals have a direct bandgap near 1.72 eV, positive birefringence ( $n_e > n_o$ ), and a large nonlinear optical coefficient.<sup>1,2</sup> They are part of the family of II-IV-V<sub>2</sub> nonlinear optical materials.<sup>3</sup> Unlike the ZnGeP<sub>2</sub> and CdSiP<sub>2</sub> crystals widely used in optical parametric oscillators to generate tunable output in the 3–6 μm region,<sup>4,5</sup> the phasematching needed for similar applications is not possible in CdGeP<sub>2</sub> crystals because of a smaller birefringence.<sup>2,4</sup> Other potential applications, however, have emerged

for CdGeP<sub>2</sub>. Optical rectification of near-infrared laser pulses generates broadband terahertz radiation<sup>6–8</sup> and doping with Mn produces room-temperature ferromagnetism suitable for spintronics.<sup>9–12</sup>

In the present paper, we use electron paramagnetic resonance (EPR), electron-nuclear double resonance (ENDOR), and optical absorption to identify and characterize intrinsic point defects (vacancies and antisites) in a CdGeP<sub>2</sub> crystal. Initially, in the as-grown crystal, the defects are in charge states that have no unpaired spins, and no EPR signals are observed. Exposing the compensated crystal to near-band-edge light while being held at low temperature converts the defects to charge states that are

17 JULY 2023 17:42:25

easily monitored with EPR. The light produces spectra from singly ionized cadmium vacancies, singly ionized germanium-on-cadmium antisites, and neutral phosphorous vacancies. Spin-Hamiltonian parameters ( $g$  and hyperfine matrices) obtained from the angular dependence of the EPR spectra are used to establish detailed models of the defects. Two photoinduced optical absorption bands observed at low temperatures are attributed to these native defects.

By including CdGeP<sub>2</sub>, our present report significantly increases the amount of experimental data in the literature describing native defects in nonlinear II-IV-P<sub>2</sub> crystals. Earlier EPR and optical absorption studies focused on defects in ZnGeP<sub>2</sub>, ZnSiP<sub>2</sub>, and CdSiP<sub>2</sub> crystals.<sup>13–30</sup> The more complete set of experimental data now available, when coupled with computational modeling efforts using advanced density-functional-theory (DFT) methods,<sup>31–37</sup> is expected to lead to a comprehensive understanding of the device-limiting intrinsic defects in these chalcopyrite materials. This, in turn, should provide guidance to crystal growers attempting to maintain stoichiometry, either during growth or with post-growth diffusion and annealing treatments.

## II. EXPERIMENTAL DETAILS

An undoped CdGeP<sub>2</sub> crystal was grown by the horizontal gradient freeze method at BAE Systems (Nashua, NH). The process previously developed at BAE Systems to grow ZnGeP<sub>2</sub> and CdSiP<sub>2</sub> crystals was followed.<sup>5,38</sup> A transparent furnace was used and the starting materials were synthesized from high-purity elements. The melting point of CdGeP<sub>2</sub> is near 800 °C.<sup>39</sup> A small rectangular-shaped crystal suitable for optical and EPR experiments was cut from the larger boule. The approximate dimensions of this crystal were 2.7 × 2.0 × 3.5 mm<sup>3</sup>, with [110], [1 $\bar{1}$ 0], and [001] directions perpendicular to the faces.

The EPR spectra were acquired with a Bruker EMX spectrometer operating near 9.39 GHz. An Oxford Instruments ESR-900 helium-gas flow system controlled the sample temperature and a Bruker NMR gaussmeter provided corrections for the small difference in the magnetic field at the sample and the Hall sensor located on a magnet pole cap. The intrinsic defects were converted to their paramagnetic charge states with either 700 or 850 nm light from an LED (Thorlabs Models M700L4 and M850L3). The approximate bandwidths (FWHM) of the LEDs were 20 and 30 nm, respectively. The concentrations of defects were obtained by comparing their spectra (intensities, linewidths, and number of lines) to a Bruker standard pitch sample. ENDOR spectra were taken with a Bruker Elexsys E-500 spectrometer operating near 9.48 GHz. Frequency modulation (at 12.5 kHz) of the radio-frequency source gave first-derivative ENDOR signals. A ThermoScientific Nicolet 8700 FTIR spectrometer and an ultra-broadband fused-silica wire-grid polarizer (Thorlabs Model WP25M-UB) were used to take optical absorption spectra in the 700 nm to 2.5 μm region. The white light source and a quartz beamsplitter were used for all wavelengths, while a silicon detector was used for wavelengths less than 900 nm and a DGTS detector was used for longer wavelengths. A cryostat from Cryo Industries (Model 110-637-DND) and a temperature controller (LakeShore Model 335) were used to obtain absorption data below room temperature.

## III. CRYSTAL STRUCTURE

The CdGeP<sub>2</sub> crystals have a tetragonal structure (space group *I42d*). Lattice constants at room temperature are given in Table I (values from CdSiP<sub>2</sub> and ZnGeP<sub>2</sub> are included for comparison).<sup>39–42</sup> There are four formulas per unit cell in A<sup>II</sup>B<sup>IV</sup>C<sub>2</sub><sup>V</sup> chalcopyrite materials. As shown in Fig. 1, each cadmium has four phosphorous neighbors, each germanium has four phosphorous neighbors, and each phosphorus has two cadmium neighbors and two germanium neighbors. Positions of the atoms in units of ( $a, a, c$ ) lattice constants are

$$\text{Cd:}(0, 0, 0), \left(0, \frac{1}{2}, \frac{1}{4}\right),$$

$$\text{Ge:}\left(0, 0, \frac{1}{2}\right), \left(0, \frac{1}{2}, \frac{3}{4}\right),$$

and

$$P:\left(u, \frac{1}{4}, \frac{1}{8}\right), \left(-u, \frac{3}{4}, \frac{1}{8}\right), \left(\frac{3}{4}, u, \frac{7}{8}\right), \left(\frac{1}{4}, -u, \frac{7}{8}\right).$$

Small rotations of the four phosphorus atoms surrounding each cadmium and germanium atom are described by the parameter  $u$  (see Ref. 28 for an illustration of this effect). These rotations are caused by the different sizes of the cadmium and germanium atoms. In an ABC<sub>2</sub> chalcopyrite crystal where the A and B atoms are the same size,  $u = 1/4$  and  $c = 2a$ . For CdGeP<sub>2</sub>, however,  $u$  is slightly greater than 1/4 and  $c$  is less than  $2a$ . Instead of being equally spaced from its four immediate neighbors, each phosphorous

**TABLE I.** Room-temperature lattice constants for CdGeP<sub>2</sub>, CdSiP<sub>2</sub>, and ZnGeP<sub>2</sub> crystals (taken from Refs. 39–42). Separation distances and angles are included. Multiplicity refers to the number of occurrences within a tetrahedron.

	Multiplicity	CdGeP <sub>2</sub>	CdSiP <sub>2</sub>	ZnGeP <sub>2</sub>
Lattice constants				
$a$ (Å)		5.740	5.680	5.46
$c$ (Å)		10.773	10.431	10.71
$u$		0.283	0.2967	0.2582
$c/a$		1.877	1.836	1.962
AP <sub>4</sub> tetrahedra (A is Cd or Zn)				
A-P (Å)	4	2.55	2.561	2.375
P-P (Å)	4	4.08	4.064	3.856
P-P (Å)	2	4.34	4.407	3.924
∠P-A-P	4	106.2°	105.0°	108.5°
∠P-A-P	2	116.3°	118.8°	111.4°
BP <sub>4</sub> tetrahedra (B is Si or Ge)				
B-P (Å)	4	2.33	2.247	2.324
P-P (Å)	4	3.81	3.674	3.792
P-P (Å)	2	3.80	3.661	3.798
∠P-B-P	4	109.5°	109.7°	109.3°
∠P-B-P	2	109.3°	109.1°	109.6°

17 JULY 2023 17:42:25

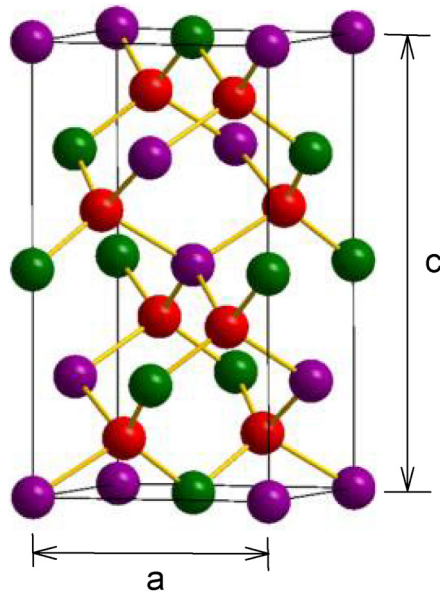


**FIG. 1.** Schematic representation of the tetrahedrally bonded CdGeP<sub>2</sub> crystal. Cadmium atoms are purple, germanium atoms are green, and phosphorous atoms are red.

atom shifts by an amount  $\Delta x = (u - 1/4)a$  along an  $a$  direction toward the two germanium neighbors and away from the two cadmium neighbors. A complete set of bond lengths and bond angles for CdGeP<sub>2</sub>, CdSiP<sub>2</sub>, and ZnGeP<sub>2</sub> is given in Table I. GeP<sub>4</sub> and SiP<sub>4</sub> units in these materials are very close to regular tetrahedra (with equal P-P separation distances and bond angles near 109.47°). The CdP<sub>4</sub> and ZnP<sub>4</sub> units, however, are distorted tetrahedra, with two of the P-P distances significantly larger than the remaining four P-P distances. Tetrahedral covalent radii (1.173, 1.128, 1.225, 1.225, and 1.405 Å for Si, P, Zn, Ge, and Cd, respectively) provided by Van Vechten and Phillips<sup>43</sup> predict, with good agreement, the experimental Cd-P, Ge-P, Si-P, and Zn-P separation distances in Table I.

Density-functional-theory (DFT) calculations of the electronic structure of CdGeP<sub>2</sub> by He *et al.*<sup>44</sup> show that Cd-P interactions are dominant at the top of the valence band and Ge-P interactions dominate the bottom of the conduction band. Specifically, the top of the valence band is formed primarily from P-3p and Cd-4p states, with a small contribution from Ge-4p states, whereas the conduction band is formed primarily from P-3p, Ge-4s, and Ge-4p states, with a small contribution from Cd-4p states.

#### IV. CADMIUM VACANCIES ( $V_{Cd}^-$ )

##### A. EPR results

Figure 2 shows the EPR spectra from singly ionized cadmium vacancies ( $V_{Cd}^-$ ) and singly ionized germanium-on-cadmium antisites ( $Ge_{Cd}^+$ ) in the CdGeP<sub>2</sub> crystal. In Fig. 2(a), the magnetic field was along the [001] direction. In Figs. 2(b) and 2(c), the field was along the [100] and [110] directions, respectively. These spectra were acquired at 60 K while the crystal was exposed to 700 nm light

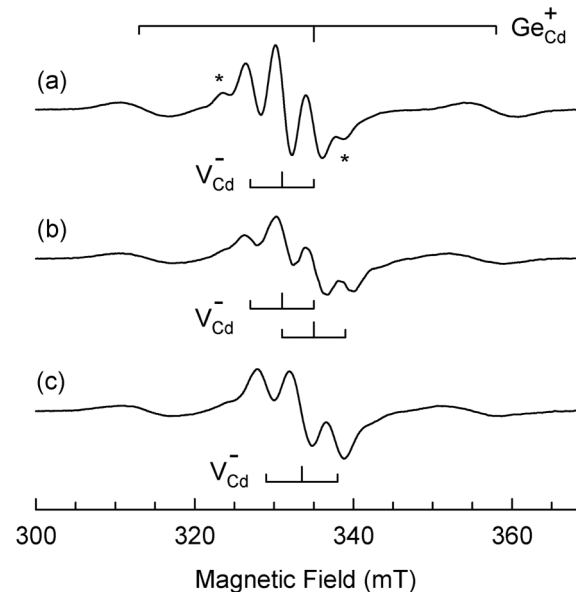


**FIG. 2.** Photoinduced EPR spectra from the singly ionized cadmium vacancy ( $V_{Cd}^-$ ) and the singly ionized germanium-on-cadmium antisite ( $Ge_{Cd}^+$ ) in a CdGeP<sub>2</sub> crystal. These spectra were taken at 60 K during exposure to 700 nm light. The microwave frequency was 9.393 GHz. (a) Magnetic field was along the [001] direction in the crystal. (b) Magnetic field was along the [100] direction. (c) Magnetic field was along the [110] direction. The two small lines identified with an asterisk (\*) in the [001] spectrum represent Cd hyperfine.

(850 nm light produced the same spectra). After removing the light, the intensities of the two spectra decreased by approximately 23% over several minutes, as electrons and holes on spatially close  $Ge_{Cd}^+$  donors and  $V_{Cd}^-$  acceptors recombined via tunneling. This left only well-separated  $Ge_{Cd}^+$  donors and  $V_{Cd}^-$  acceptors to contribute to the spectra. Although the remaining  $Ge_{Cd}^+$  donors and  $V_{Cd}^-$  acceptors are stable in the dark at 60 K, they were destroyed in a few seconds when the crystal was exposed at this temperature to 1064 nm laser light. In Fig. 2, the EPR lines from cadmium vacancies are between 325 and 341 mT. The antisite donors have outer lines near 313 and 355 mT and a third centerline near 334 mT under the cadmium vacancy signals. Lines assigned to the defects are identified in the figure by “stick” diagrams. An estimate of the concentration of  $V_{Cd}^-$  acceptors in Fig. 2 is  $1.5 \times 10^{18} \text{ cm}^{-3}$ . A similar number of  $Ge_{Cd}^+$  donors are present.

There were no detectable EPR signals before exposure to light, indicating that the cadmium vacancies and antisites are in doubly ionized charge states in the as-grown crystal. The following are possible mechanisms that allow the 700 or 850 nm light at 60 K (as in Fig. 2) to produce  $V_{Cd}^-$  acceptors and  $Ge_{Cd}^+$  donors. The light may (1) move electrons from the valence band to the conduction band with the “free” electrons and holes then trapped at  $Ge_{Cd}^{2+}$  donors and  $V_{Cd}^{2-}$  acceptors, (2) move electrons from  $V_{Cd}^{2-}$  acceptors to the conduction band with the electrons trapped at  $Ge_{Cd}^{2+}$  donors, (3) move electrons from the valence band to  $Ge_{Cd}^{2+}$  donors with the holes trapped at  $V_{Cd}^{2-}$  acceptors, or (4) move electrons

17 July 2023 17:42:25

from the valence band to  $V_{\text{P}}^+$  donors (see Sec. V) with the electrons transferring to deeper  $\text{Ge}_{\text{Cd}}^{2+}$  donors and the holes trapped at  $V_{\text{Cd}}^{2-}$  acceptors.

In Fig. 2(a), the  $S = 1/2$  EPR spectrum from the singly ionized cadmium vacancies ( $V_{\text{Cd}}^-$ ) consists of one set of three lines with relative intensities of 1:2:1. Equal hyperfine interactions with two of the phosphorous nuclei adjacent to the vacancy are responsible for the three lines (the  $^{31}\text{P}$  nuclei have an  $I = 1/2$  spin and are 100% abundant). This establishes a model for the  $V_{\text{Cd}}^-$  acceptor that has the unpaired electron shared by two phosphorous neighbors and not one or four phosphorous neighbors. Similar three-line EPR spectra have been reported for singly ionized zinc vacancies ( $V_{\text{Zn}}^-$ ) in  $\text{ZnGeP}_2$  and  $\text{ZnSiP}_2$  crystals<sup>13,26</sup> and cadmium vacancies ( $V_{\text{Cd}}^-$ ) in  $\text{CdSiP}_2$  crystals.<sup>28</sup> [Note: The small outer lines marked with asterisks in Fig. 2(a) are part of the  $V_{\text{Cd}}^-$  spectrum. They are tentatively assigned to hyperfine interactions with nearby Cd nuclei.] In Fig. 2(b), the  $V_{\text{Cd}}^-$  spectrum consists of two sets of three lines. In Fig. 2(c), the spectrum consists of one set of three lines. The complete angular dependence of the EPR spectrum from  $V_{\text{Cd}}^-$  acceptors is shown in Fig. 3. Spectra were taken at various angles as the direction of the static magnetic field was rotated from [100] to [001] and from [001] to [110]. Overlapping EPR lines were not resolved at some of the angles because of the large linewidths ( $\geq 2.0$  mT).

As illustrated in Fig. 4, there are four crystallographically equivalent orientations (or sites) adjacent to a cadmium vacancy for the pairs of phosphorous atoms that share the unpaired spin. The  $\text{P}_1$ - $\text{P}_2$  pair is the labeled site 1, the  $\text{P}_2$ - $\text{P}_3$  pair is site 2, the  $\text{P}_3$ - $\text{P}_4$  pair is site 3, and the  $\text{P}_4$ - $\text{P}_1$  pair is site 4. The unpaired spin is not shared by  $\text{P}_1$  and  $\text{P}_3$  atoms or  $\text{P}_2$  and  $\text{P}_4$  atoms. This preferential trapping of the hole on one of the four adjacent pairs,

instead of all six, is a result of the compression of the lattice along the  $c$  axis (i.e.,  $c/2a$  being less than 1). As seen in Table I, the  $\text{P}_1$ - $\text{P}_3$  and  $\text{P}_2$ - $\text{P}_4$  separations are larger than the separations of the other four pairs of phosphorous atoms surrounding the cadmium vacancy. The increased separation makes these two pairs energetically less favorable for trapping the hole. When rotating from [100] to [001] in Fig. 3, the spectra from sites 1 and 3 are degenerate and give one set of three hyperfine lines (the black set of lines), whereas the spectra from sites 2 and 4 are not degenerate, with each giving a set of three lines (the red set and the blue set, respectively). For rotation from [001] to [110] in Fig. 3, the spectra from sites 1 and 4 are equivalent and give the blue set of lines and the spectra from sites 2 and 3 are equivalent and give the red set of lines.

The following spin-Hamiltonian is used to analyze the  $V_{\text{Cd}}^-$  angular dependence in Fig. 3. Electron Zeeman, hyperfine, and nuclear Zeeman terms are included,

$$H = \beta \mathbf{S} \cdot \mathbf{g} \cdot \mathbf{B} + \mathbf{I}_1 \cdot \mathbf{A}_1 \cdot \mathbf{S} + \mathbf{I}_2 \cdot \mathbf{A}_2 \cdot \mathbf{S} - g_N \beta_N (\mathbf{I}_1 + \mathbf{I}_2) \cdot \mathbf{B}. \quad (1)$$

Subscripts 1 and 2 represent the two equivalent phosphorous nuclei. The principal-axis directions of the  $\mathbf{g}$ ,  $\mathbf{A}_1$ , and  $\mathbf{A}_2$  matrices are collinear, and the  $\mathbf{A}_1$  and  $\mathbf{A}_2$  matrices have the same principal values. Euler angles ( $\alpha$ ,  $\beta$ , and  $\gamma$ ), defined in the EasySpin EPR simulation program<sup>45,46</sup> and earlier by Rose<sup>47</sup> and Arfken and Weber<sup>48</sup> are used to describe the directions of the principal axes. Referring to site 2 in Fig. 4, a principal axis labeled  $x$  is in the (010) plane (near the  $[10\bar{1}]$  direction), a second principal axis labeled  $y$  is along the  $[010]$  direction, and a third axis labeled  $z$  is near the  $[101]$  direction in the (010) plane. The  $z$  principal axis direction for this site is close to the line from  $\text{P}_3$  to  $\text{P}_2$ . There are seven parameters to

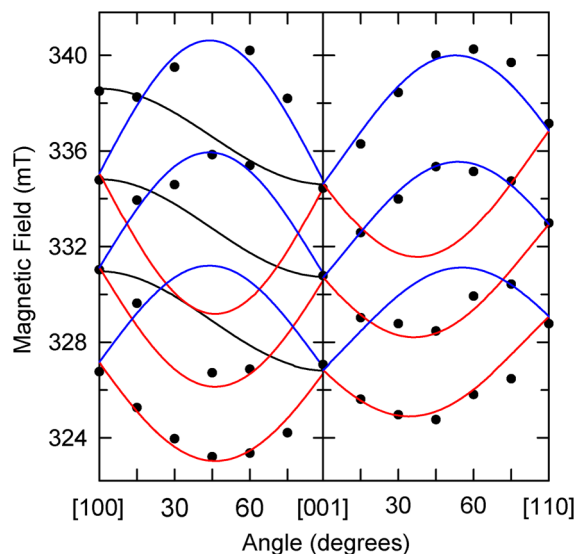


**FIG. 3.** Angular dependence of the EPR spectrum from singly ionized cadmium vacancies ( $V_{\text{Cd}}^-$ ). The discrete points are experimental data taken at 60 K. “Best fit” parameters in Table II were used to generate the solid lines.

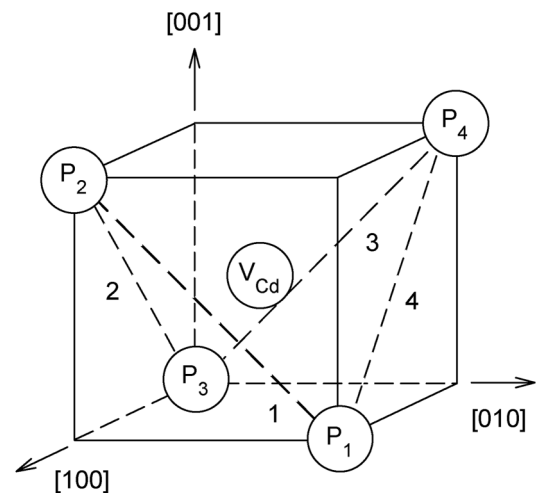


**FIG. 4.** Model of the singly ionized cadmium vacancy ( $V_{\text{Cd}}^-$ ) in  $\text{CdGeP}_2$ . The unpaired spin is equally shared by two phosphorous atoms adjacent to the vacancy. The four possible orientations of the trapped hole (labeled 1 through 4) correspond to four equivalent pairs of phosphorus atoms with shorter separation distances.

**TABLE II.** Spin-Hamiltonian parameters for the singly ionized cadmium vacancy ( $V_{\text{Cd}}^-$ ) in  $\text{CdGeP}_2$ . The directions of the principal axes are given for site 2 in Fig. 4. The Euler angles ( $\alpha$ ,  $\beta$ , and  $\gamma$ ) for the collinear  $\mathbf{g}$  and  $\mathbf{A}$  matrices are  $0^\circ$ ,  $44^\circ$ , and  $0^\circ$ , respectively (see Ref. 45 for definitions of these angles). Uncertainties are estimated to be  $\pm 0.001$  for the  $g$  values,  $\pm 2.0$  MHz for the  $A$  values, and  $\pm 2^\circ$  for the angles.

	Principal values	Principal-axis directions
<b><math>\mathbf{g}</math> matrix</b>		
$g_x$	1.9956	$134^\circ$ from [001], in the (010) plane
$g_y$	2.0023	Along [010]
$g_z$	2.0556	$44^\circ$ from [001], in the (010) plane
<b><math>\mathbf{A}_1</math> and <math>\mathbf{A}_2</math> matrices</b>		
$A_x$	131.4 MHz	$134^\circ$ from [001], in the (010) plane
$A_y$	107.0 MHz	Along [010]
$A_z$	88.6 MHz	$44^\circ$ from [001], in the (010) plane

be extracted from the angular dependence (three principal values of the  $\mathbf{g}$  matrix, three principal values of the  $\mathbf{A}$  matrices, and the angle  $\beta$  between the  $z$  principal axis of the matrices and the [001] direction).

The spin-Hamiltonian in Eq. (1) was rewritten as an  $8 \times 8$  matrix, and values for the seven parameters were determined using a least-squares fitting program. Input data consisted of 40 of the experimental line positions in Fig. 3 and their corresponding microwave frequencies. The energy eigenvalues of the Hamiltonian were repeatedly calculated as the seven parameters were systematically varied. In the fitting program, the predicted line positions (obtained from the eigenvalues) were compared to the measured line positions. Table II contains the best-fit values for the seven parameters that describe the singly ionized cadmium vacancy  $V_{\text{Cd}}^-$  in  $\text{CdGeP}_2$ . These final parameters were used to generate the solid curves in Fig. 3. Our  $\mathbf{g}$  and  $\mathbf{A}$  parameters for the cadmium vacancy are similar to parameters previously reported for zinc vacancies in  $\text{ZnGeP}_2$  and  $\text{ZnSiP}_2$  and the cadmium vacancy in  $\text{CdSiP}_2$ .<sup>15,26,28</sup>

## B. ENDOR results

Electron-nuclear double resonance (ENDOR) experiments<sup>49,50</sup> provide a high-resolution survey of a defect's hyperfine interactions, often revealing couplings that are not resolved in the EPR spectra. In ENDOR experiments, the magnetic field is held constant at the center of an EPR line while a radio frequency (rf) source is swept at a constant rate through frequencies of interest. ENDOR signals occur at frequencies where the rf "flips" a nuclear spin coupled to the defect's unpaired electron spin. For an  $S = 1/2$ ,  $I = 1/2$  spin system, the selection rules give, to first order, pairs of ENDOR lines at rf frequencies  $f_1$  and  $f_2$ ,

$$f_{1,2} = A/2 \pm \nu_N \text{ (if } \nu_N \text{ is less than } A), \quad (2)$$

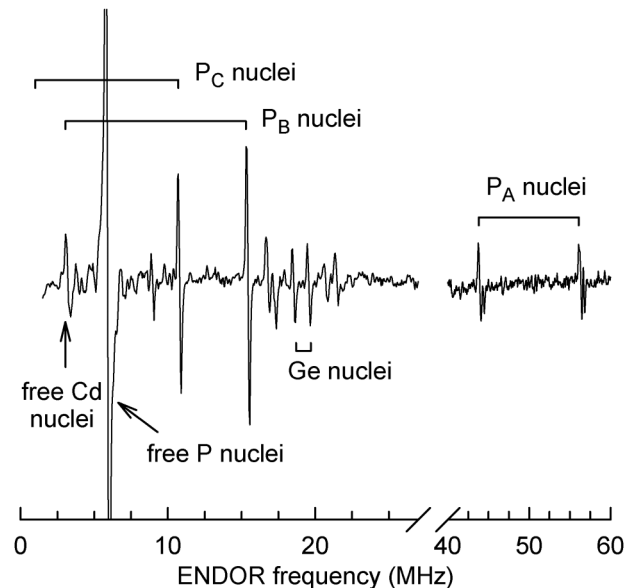
$$f_{1,2} = \nu_N \pm A/2 \text{ (if } \nu_N \text{ is greater than } A). \quad (3)$$

The "free" nuclear resonance frequency  $\nu_N$  is  $\mu\beta_N B/hI$ , where  $I$  is the nuclear spin,  $\beta_N$  is the nuclear magneton,  $\mu$  is the nuclear

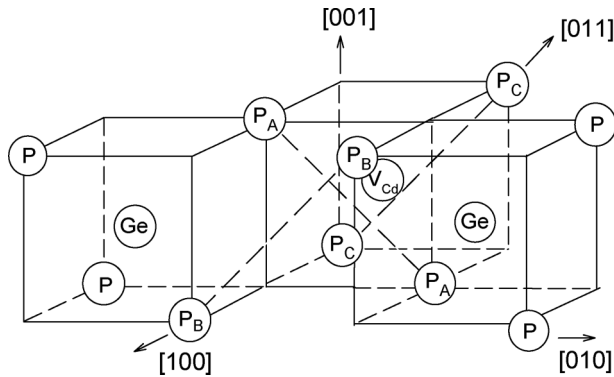
magnetic dipole moment in units of the nuclear magneton,  $h$  is Planck's constant, and  $B$  is the magnitude of the magnetic field. In experiments, observing a pair of ENDOR lines (at  $f_1$  and  $f_2$ ) provides values for  $\nu_N$  and  $A$ , with  $\nu_N$  identifying the responsible nucleus and  $A$  representing the hyperfine coupling.

Figure 5 shows an ENDOR spectrum from  $V_{\text{Cd}}^-$  acceptors in  $\text{CdGeP}_2$ , taken at 17 K after exposing the crystal to 700 nm light at this temperature. The microwave frequency was 9.484 GHz, and the magnetic field was along the [110] direction and fixed at 342.4 mT, a position that corresponds to the highest field EPR line in Fig. 2(c). Using this fixed value of the magnetic field and the known nuclear magnetic moments from Ref. 51, the corresponding free nuclear resonance frequencies  $\nu_N$  are 5.907, 0.510, 3.105, and 3.248 MHz for the  $^{31}\text{P}$ ,  $^{73}\text{Ge}$ ,  $^{111}\text{Cd}$ , and  $^{113}\text{Cd}$  nuclei, respectively. In Fig. 5, lines from three  $^{31}\text{P}$  interactions and one  $^{73}\text{Ge}$  interaction are present as well as "distant" ENDOR lines from uncoupled  $^{111,113}\text{Cd}$  and  $^{31}\text{P}$  nuclei. Figure 6 shows the locations around the Cd vacancy of the nuclei responsible for the  $^{73}\text{Ge}$  interaction and the three  $^{31}\text{P}$  interactions. The phosphorous sites are labeled  $P_A$ ,  $P_B$ , and  $P_C$ .

The pair of ENDOR lines, near 44.07 and 56.49 MHz in Fig. 5, corresponds to the case described by Eq. (2) and is due to  $^{31}\text{P}$  nuclei at  $P_A$  positions in Fig. 6. These two atoms share much of the unpaired spin and are responsible for the resolved hyperfine observed in the EPR spectra of the  $V_{\text{Cd}}^-$  acceptor (see Fig. 2). The small barely resolved 0.4 MHz splitting within each of these lines in the high-frequency region of Fig. 5 is a result of the indirect coupling of equivalent  $^{31}\text{P}$  nuclei.<sup>49</sup> The lines are separated by



**FIG. 5.** ENDOR spectrum of the singly ionized cadmium vacancy ( $V_{\text{Cd}}^-$ ) in  $\text{CdGeP}_2$ . The temperature was 17 K, and the microwave frequency was 9.484 GHz. The magnetic field was along the [110] direction and fixed at 342.4 mT. Labels identify the responsible nuclei.



**FIG. 6.** Neighbors of the cadmium vacancy in CdGeP<sub>2</sub>. The cadmium vacancy is in the rear center “cube,” while left and right front “cubes” have germanium atoms at their centers. Three pairs of phosphorous nuclei (P<sub>A</sub>, P<sub>B</sub>, and P<sub>C</sub>) and one pair of germanium nuclei share the unpaired spin and contribute to the ENDOR spectrum in Fig. 5.

12.42 MHz, which is only slightly greater than the  $2\nu_N$  value of 11.81 MHz for the <sup>31</sup>P nuclei. Second-order effects resulting from a large A value (greater than 100 MHz) are responsible for the increased separation.<sup>49</sup> The ENDOR lines, at 15.44 and 10.80 MHz in Fig. 5, are caused by <sup>31</sup>P nuclei at sites labeled P<sub>B</sub> and P<sub>C</sub>, respectively, in Fig. 6. These assignments are supported by an earlier ENDOR study of V<sub>Zn</sub><sup>-</sup> acceptors in ZnGeP<sub>2</sub>.<sup>16</sup> The <sup>31</sup>P line at 15.44 MHz is part of a pair described by Eq. (2), with an A value near 23.63 MHz. Its companion line near 3.5 MHz is not clearly seen in Fig. 5 because of partial overlap from the uncoupled <sup>111,113</sup>Cd nuclei. The <sup>31</sup>P line at 10.80 MHz is part of a pair described by Eq. (3), with an A value near 9.79 MHz. This places its companion line near 1.00 MHz and, thus, is below the range of the rf sweep in Fig. 5.

The pair of ENDOR lines at 18.52 and 19.58 MHz in Fig. 5 are due to <sup>73</sup>Ge nuclei (7.76% natural abundance) located at the two Ge sites shown in Fig. 6. The lines are described by Eq. (2) where  $\nu_N$  is less than A. Unlike <sup>31</sup>P and <sup>111,113</sup>Cd nuclei with nuclear spins  $I = 1/2$ , the <sup>73</sup>Ge nuclei have a nuclear spin  $I = 9/2$  and are expected to exhibit nuclear electric quadrupole splittings in an ENDOR spectrum. Only the  $m_I = +1/2$  to  $m_I = -1/2$  transition for the two values of  $M_S$ , however, are seen in Fig. 5 because either the electric field gradient at the Ge nucleus is too small to produce measurable splittings or the quadrupole-split lines are too broad to observe. The two lines are separated by 1.06 MHz, which is only slightly greater than the  $2\nu_N$  value of 1.02 MHz for the <sup>73</sup>Ge nuclei (when the magnetic field is 342.4 mT). The A value obtained from the mid-point of the pair of Ge lines is 38.1 MHz. Nuclei responsible for additional ENDOR lines in Fig. 5, near 17 and 21 MHz, are not identified in the present study.

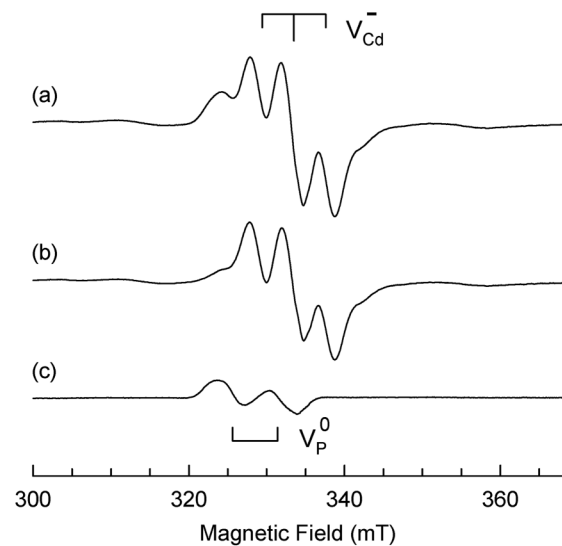
## V. PHOSPHOROUS VACANCIES (V<sub>P</sub><sup>0</sup>)

Figure 7 shows EPR spectra taken at 18 K from the CdGeP<sub>2</sub> crystal. The microwave frequency was 9.392 GHz, and the magnetic field was along the [110] direction. The spectrum in Fig. 7(a) was

obtained with 700 nm light on the crystal. The light was then removed and the spectrum in Fig. 7(b) was taken within a few seconds. In Fig. 7(a), signals from both singly ionized cadmium vacancies (V<sub>Cd</sub><sup>-</sup>) and neutral phosphorous vacancies (V<sub>P</sub><sup>0</sup>) are present as well as lines from germanium-on-cadmium antisites (Ge<sub>Cd</sub><sup>+</sup>). [Note: The V<sub>Cd</sub><sup>-</sup> acceptors and the Ge<sub>Cd</sub><sup>+</sup> donors are easily saturated with microwave power at 18 K because of long spin-lattice relaxation times. The V<sub>P</sub><sup>0</sup> donors, with much shorter relaxation times, are not saturated at this temperature.]

After removing the 700 nm light, all the neutral phosphorous vacancies quickly decay at 18 K and only the V<sub>Cd</sub><sup>-</sup> and Ge<sub>Cd</sub><sup>+</sup> spectra are left in Fig. 7(b). A small portion of these V<sub>Cd</sub><sup>-</sup> acceptors and Ge<sub>Cd</sub><sup>+</sup> donors also decayed when the light was removed, similar to the decrease that occurred at 60 K after removing the light (see Sec. IV A). Two possible mechanisms could explain the decay of neutral phosphorous vacancies at 18 K. If they are sufficiently close to V<sub>Cd</sub><sup>-</sup> acceptors, then direct donor–acceptor recombination could account for the decay of V<sub>P</sub><sup>0</sup> donors. It is also possible that V<sub>P</sub><sup>0</sup> donors are shallow and revert to singly ionized V<sub>P</sub><sup>+</sup> donors at 18 K by thermally releasing an electron to the conduction band. The report by Höglund *et al.*<sup>52</sup> that the neutral phosphorous vacancy in GaP has a state close to the conduction band supports the second mechanism.

To isolate the spectrum from the V<sub>P</sub><sup>0</sup> donors in CdGeP<sub>2</sub>, the difference spectrum in Fig. 7(c) was generated by subtracting the spectrum in Fig. 7(b) from the spectrum in Fig. 7(a). Before subtraction, the spectrum in Fig. 7(b) was multiplied by a factor of 1.2 to account for the decrease in the number of V<sub>Cd</sub><sup>-</sup> acceptors when



**FIG. 7.** EPR spectra from CdGeP<sub>2</sub>, taken at 18 K with the magnetic field along the [110] direction. (a) Spectrum taken with 700 nm light on the crystal. (b) Spectrum taken immediately after removing the 700 nm light. (c) Difference spectrum, generated by subtracting the “after light” spectrum from the “with light” spectrum. The difference spectrum contains two EPR lines from the neutral phosphorous vacancy (V<sub>P</sub><sup>0</sup>).

17 July 2023 17:42:25

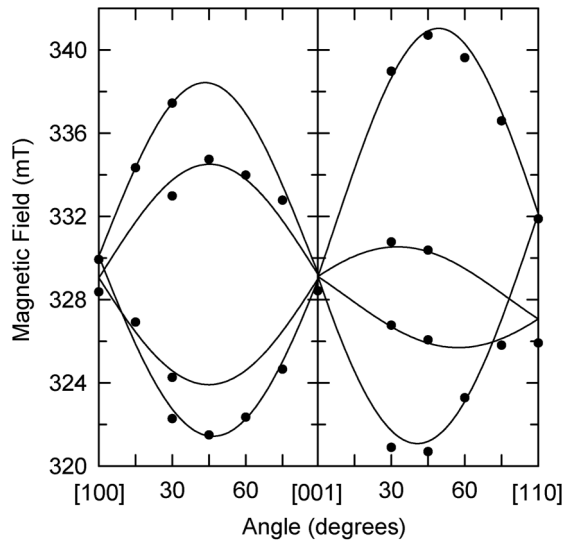


**FIG. 8.** Angular dependence of the EPR spectrum from the neutral phosphorous vacancy ( $V_p^0$ ) in  $CdGeP_2$ . The discrete points are experimental data obtained from “difference” spectra. The solid lines are generated using the “best fit” parameters in Table III.

the light was removed. For this [110] orientation of the magnetic field, the difference spectrum in Fig. 7(c) contains two equally intense lines from the  $V_p^0$  donors, identified by the lower stick diagram. The concentration of  $V_p^0$  donors in this spectrum is approximately  $8.7 \times 10^{16} \text{ cm}^{-3}$ . This concentration of photoinduced phosphorous vacancies is a factor of five less than the concentration of photoinduced cadmium vacancies in Fig. 7(a). These results, however, do not necessarily suggest that there are fewer phosphorous vacancies in our crystal, as not all the vacancies may have been converted to their paramagnetic form.

The angular dependence of the  $V_p^0$  EPR spectrum is shown in Fig. 8 for rotation of the static magnetic field from [100] to [001] and from [001] to [110]. There are four distinguishable orientations of the defect. At each angle where data were obtained, a spectrum was first taken with 700 nm light on, then a spectrum was taken after removing the light, and finally, a difference spectrum was generated to identify the  $V_p^0$  lines. Large linewidths and overlapping lines prevented usable data from being acquired at some of the angles. Since the EPR spectrum showed no resolved hyperfine, an  $S = 1/2$  spin-Hamiltonian containing only an electron Zeeman term ( $H = \beta S \cdot g \cdot B$ ) was used to analyze the angular dependence in Fig. 8. The  $g$  matrix has six independent parameters, three principal values and three Euler angles ( $\alpha$ ,  $\beta$ , and  $\gamma$ ) that describe the directions of the principal axes. After writing the spin Hamiltonian as a  $2 \times 2$  matrix, values for these parameters were determined using a least-squares fitting program. Input data consisted of the 30 experimental line positions in Fig. 8 and their corresponding microwave frequencies. Table III contains the best-fit values for the parameters that describe the neutral phosphorous vacancy ( $V_p^0$ ). These parameters were used to generate the solid curves in Fig. 8.

**TABLE III.** The  $g$  matrix for the neutral phosphorous vacancy ( $V_p^0$ ) in  $CdGeP_2$ . Euler angles ( $\alpha$ ,  $\beta$ , and  $\gamma$ ) for the  $g$  matrix are  $62.7^\circ$ ,  $41.2^\circ$ , and  $-5.7^\circ$ , respectively (see Ref. 45). Polar and azimuthal angles ( $\theta$  and  $\phi$ ) are also used to describe the principal-axis directions. Uncertainties are estimated to be  $\pm 0.001$  for the  $g$  values and  $\pm 2^\circ$  for the angles.

Principal values		Principal-axis directions	
		$\theta$	$\phi$
$g_1$	1.967	$49.2^\circ$	$55.2^\circ$
$g_2$	2.052	$86.0^\circ$	$148.7^\circ$
$g_3$	2.092	$41.1^\circ$	$243.3^\circ$
Line from Ge atom to		$54.7^\circ$	$49.0^\circ$
P vacancy			

To allow the principal axes to be more easily visualized, the directions are expressed in polar and azimuthal angles in Table III. The polar angle  $\theta$  is defined relative to [001], and the azimuthal angle  $\phi$  is defined relative to [100] with a positive rotation from [100] toward [010] in the plane perpendicular to [001]. Our  $g$ -matrix parameters for the phosphorous vacancy in  $CdGeP_2$  are similar to those obtained for the phosphorous vacancy in  $ZnGeP_2$ .<sup>14</sup> In  $ZnSiP_2$  and  $CdSiP_2$ , only the  $g_c$  value was reported for the phosphorous vacancy.<sup>26,28</sup>

In a DFT study, Jiang *et al.*<sup>33</sup> predicted that the unpaired spin associated with the neutral phosphorous vacancy ( $V_p^0$ ) in  $ZnGeP_2$ <sup>33</sup> is shared by the two neighboring Ge atoms. These investigators also found that the formation of the neutral anion vacancy was accompanied by a significant relaxation of the surrounding lattice, with the Zn atoms moving away from the vacancy and the Ge atoms moving toward the vacancy. In  $CdGeP_2$ , the experimentally determined directions of the principal axes of the  $g$  matrix in Table III suggest that the phosphorous vacancy’s unpaired spin is localized on one adjacent Ge atom. The direction of the principal axis associated with  $g_1$  is close to the line from a Ge atom to the center of the vacancy (i.e., the direction of the  $sp^3$  lobe extending out from the Ge atom). The polar and azimuthal angles ( $\theta$  and  $\phi$ ) for this latter direction in the unrelaxed lattice are included in Table III. If the unpaired spin were shared by two adjacent Ge atoms, one of the principal axes should be close to the line joining the two Ge atoms. None of the  $g$ -matrix principal-axis directions, however, is close to the Ge–Ge internuclear axis.

## VI. GERMANIUM-ON-CADMIUM ANTISITES ( $Ge_{Cd}^+$ )

Figure 2 shows the photoinduced EPR spectrum from the singly ionized germanium-on-cadmium antisite ( $Ge_{Cd}^+$ ) in the  $CdGeP_2$  crystal. Similar spectra have been reported for cation antisite donors (group IV atoms on group II sites) in  $ZnGeP_2$ ,  $ZnSiP_2$ , and  $CdSiP_2$  crystals.<sup>17,26,28</sup> In the II-IV- $P_2$  chalcopyrites, these antisite donors are easily saturated (especially at lower temperatures), and, thus, are best observed with low microwave power. The  $Ge_{Cd}^+$  spectra in Fig. 2 consist of three lines caused by equal hyperfine interactions with two adjacent phosphorous nuclei (the center line is under the  $V_{Cd}^-$  spectrum). Just as with the  $V_{Cd}^-$  spectra in Sec. IV, equal interactions give ratios of 1:2:1 for the lines. The

17 JULY 2023 17:42:25

germanium atom is smaller than the cadmium atom it replaces, thus allowing relaxation of the surrounding lattice. A similar situation occurs in CdSiP<sub>2</sub> where the silicon atom is considerably smaller than the cadmium atom. It remains unclear, however, as to why the unpaired spin is primarily localized on two phosphorous neighbors, instead of being equally shared by all four phosphorous neighbors in these antisite defects. In ZnGeP<sub>2</sub>, the zinc atom is the same size as the germanium atom, but the unpaired spin in the Ge<sub>Zn</sub><sup>+</sup> donor is still shared by only two adjacent phosphorous atoms.<sup>17</sup> In Fig. 2, the widths of the Ge<sub>Cd</sub><sup>+</sup> lines are approximately 6.1 mT. Much of this large width is unresolved hyperfine caused by overlap of the unpaired spin onto the neighboring atoms.

The EPR spectrum from the Ge<sub>Cd</sub><sup>+</sup> donors exhibits very little angular dependence (see Fig. 2), and a detailed analysis of *g* and hyperfine parameters was not attempted. With the magnetic field along the [001] direction, the *g* value is 1.996 and the hyperfine parameter for each of the two primary <sup>31</sup>P nuclei (spacing between adjacent lines) is 615 MHz. For the [100] direction, these values are 2.001 and 579 MHz. For the [110] direction, they are 2.004 and 568 MHz. Slightly smaller hyperfine values were reported for Ge<sub>Zn</sub><sup>+</sup> and Si<sub>Cd</sub><sup>+</sup> donors<sup>17,28</sup> in ZnGeP<sub>2</sub> and CdSiP<sub>2</sub>, and values approximately 50% smaller were reported for the Si<sub>Zn</sub><sup>+</sup> donor<sup>26</sup> in ZnSiP<sub>2</sub>.

For completeness, we draw attention to another antisite donor (a group V atom on group IV sites) that was observed with EPR in an early study of ZnGeP<sub>2</sub> and CdSiP<sub>2</sub> crystals.<sup>53</sup> These P<sub>Ge</sub><sup>0</sup> and P<sub>Si</sub><sup>0</sup> donors (i.e., PP<sub>4</sub> clusters) have a large hyperfine interaction (~2380 MHz) with the center phosphorous atom and have smaller equal hyperfine interactions (~244 MHz) with the four surrounding phosphorous atoms. Their neutral charge state was formed at low temperature with near-band-edge light (and decayed in a few minutes at 20 K after removing the light). The P<sub>Ge</sub><sup>0</sup> and P<sub>Si</sub><sup>0</sup> donors have not been detected in crystals grown in recent years by the horizontal gradient freeze technique.

## VII. OPTICAL ABSORPTION

As initially described by Shay *et al.*,<sup>1</sup> CdGeP<sub>2</sub> crystals have a direct energy gap near 1.72 eV at room temperature, corresponding to a transition from the highest of the three valence bands to the conduction band. Selection rules for this transition require that light polarized with *E* || *c* is preferentially absorbed (i.e., the optical absorption coefficient when approaching the edge from the long wavelength side is larger for *E* || *c* than for *E* ⊥ *c*). Absorption spectra show an apparent shift of the band edge when using different polarizations of the probe light. Shay *et al.*<sup>1</sup> also confirmed that the energy gap widens when the crystal is cooled below room temperature, an important behavior for the present study, when 700 nm (1.77 eV) light is used to produce EPR spectra.

Figure 9(a) shows the optical absorption spectra obtained at 80 K from the CdGeP<sub>2</sub> crystal. Polarized light (*E* ⊥ *c*) was used. Corrections were not made for reflection losses. A spectrum was taken before exposing the crystal to 850 nm light (only light from the FTIR spectrometer was present). Then a spectrum was taken with 850 nm light from the LED on the crystal. The additional 850 nm light further increased the absorption across the region from 2.0 μm to 700 nm. We attribute much of the absorption seen in this region before applying the LED to the effects of the

spectrometer's white light source. Figure 9(b) shows the difference between the "with 850 nm" and the "before" spectra. This difference spectrum is composed of two broad overlapping bands, as illustrated by green and blue curves in the figure. The green curve is a simulation that has a Gaussian shape with a peak at 1.18 eV (1.05 μm). It was generated by matching the simulation to the difference curve in the 0.7–1.0 eV region. The blue curve in Fig. 9(b), with a peak near 1.64 eV (756 nm), was then obtained by subtracting the green curve from the difference curve. Although not shown, a less intense absorption band is seen near 2.0 μm with light-polarized *E* || *c*.

The two photoinduced optical absorption bands in Fig. 9(b), at 1.05 μm and 756 nm, are associated with native point defects. In ZnGeP<sub>2</sub>, a broad band peaking near 1.2 μm has been attributed to singly ionized zinc vacancies,<sup>18,20</sup> and in CdSiP<sub>2</sub>, several broad bands peaking in the 800 nm to 1.0 μm region have been attributed to singly ionized silicon vacancies.<sup>29</sup> By analogy with ZnGeP<sub>2</sub>, we suggest that the 1.05 μm band in CdGeP<sub>2</sub> is a transition associated with singly ionized cadmium vacancies (EPR shows that cadmium

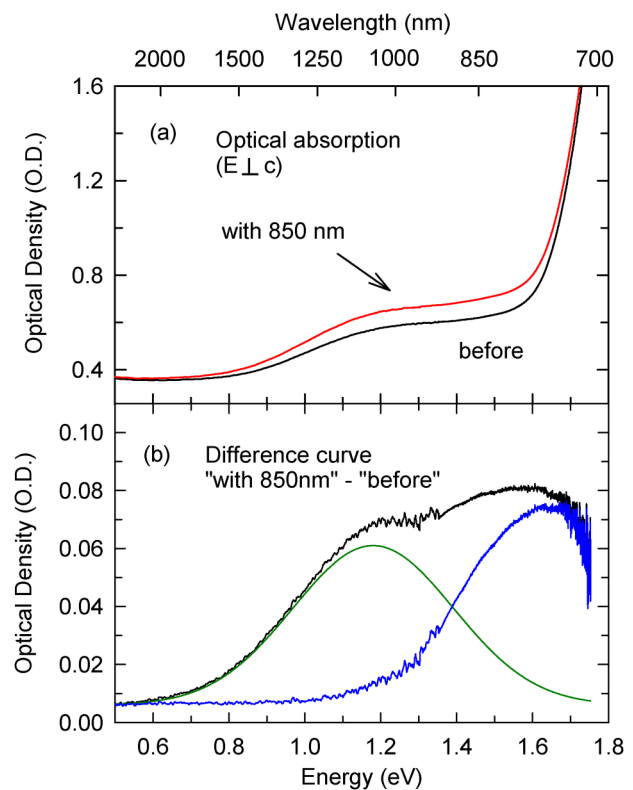


**FIG. 9.** Photoinduced optical absorption in CdGeP<sub>2</sub>, taken at 80 K with light polarized *E* ⊥ *c*. (a) These spectra were taken before and with 850 nm light incident on the crystal. (b) Difference spectrum obtained by subtracting the "before" spectrum from the "with 850 nm light" spectrum. The difference spectrum contains two absorption bands. The green band is a Gaussian fit peaking near 1.05 μm. The blue band, peaking near 756 nm, represents remaining absorption after the green band is subtracted from the difference spectrum.

17 July 2023 17:42:25

vacancies are the dominant acceptors in CdGeP<sub>2</sub>). Possible models are either an intracenter transition from the ground state to a localized excited state of the V<sub>Cd</sub><sup>-</sup> acceptor or an acceptor-to-donor transition involving V<sub>Cd</sub><sup>-</sup> acceptors and Ge<sub>Cd</sub><sup>+</sup> donors. The defect(s) responsible for the 756 nm band in CdGeP<sub>2</sub> are not identified in the present study.

## VII. AN OVERVIEW OF NATIVE DEFECTS IN ZnGeP<sub>2</sub>, ZnSiP<sub>2</sub>, CDSiP<sub>2</sub>, AND CdGeP<sub>2</sub>

There is a consistency among the native defects observed in various II-IV-P<sub>2</sub> chalcopyrites. Crystals grown for nonlinear optical applications are usually compensated, with group II and group IV vacancies being the dominant acceptors and antisites (group IV atoms on group II sites) and P vacancies being the dominant donors. The energies of formation for these defects have been calculated by Jiang *et al.*<sup>33</sup> Low levels of unintentional impurities such as Fe, Mn, Ni, and Cu, coming from starting materials, are also often present but normally play minor roles.

**Group II vacancies:** These vacancies are very common in the II-IV-P<sub>2</sub> chalcopyrites. They are present in the as-grown crystals as doubly ionized acceptors but are converted to paramagnetic singly ionized acceptors (V<sub>Zn</sub><sup>-</sup> and V<sub>Cd</sub><sup>-</sup>) by exposure at low temperature to near-band-edge light. When there is an insufficient concentration of donors, a portion of the group II vacancies will be in the singly ionized state in the as-grown crystals. The singly ionized acceptors have their unpaired spin localized on two of the phosphorous atoms adjacent to the vacancy. This gives a characteristic three-line hyperfine spectrum that is easily monitored with EPR at low temperatures. An intracenter transition (ground state to a localized excited state) of these singly ionized acceptors is responsible for a broad optical absorption band peaking near 1.0 μm.

**Group IV vacancies:** These vacancies are less common in the II-IV-P<sub>2</sub> crystals. The V<sub>Si</sub><sup>-</sup> acceptors are seen with EPR in as-grown CdSiP<sub>2</sub> crystals, and their concentration can often be increased by illuminating at low temperatures with near-band-edge light. In contrast, the V<sub>Ge</sub><sup>-</sup> acceptors are not seen in as-grown ZnGeP<sub>2</sub> crystals but have been formed by displacement events when a crystal is irradiated at room temperature with 2 MeV electrons. Thus far, there have been no reports of group IV vacancies in ZnSiP<sub>2</sub> and CdGeP<sub>2</sub> crystals. Singly ionized group IV vacancies have a characteristic five-line EPR hyperfine spectrum because the unpaired spin is equally shared by the four phosphorous neighbors. In CdSiP<sub>2</sub>, the V<sub>Si</sub><sup>-</sup> acceptors are responsible for broad optical absorption bands peaking near 800 nm and 1.0 μm.

**Antisite donors:** The group-IV-on-group-II antisites are a major donor in II-IV-P<sub>2</sub> crystals, being seen with large concentrations in all the materials studied thus far. Because of the presence of acceptors, these antisites are usually doubly ionized (Ge<sub>Zn</sub><sup>2+</sup>, Si<sub>Zn</sub><sup>2+</sup>, Si<sub>Cd</sub><sup>2+</sup>, and Ge<sub>Cd</sub><sup>2+</sup>) in the as-grown crystals. They are converted to paramagnetic singly ionized donors with near-band-edge light, as electrons move from acceptors to donors. The unpaired spin is equally shared by two of the adjacent phosphorous atoms, thus giving a widely separated three-line EPR hyperfine spectrum that has very little angular dependence.

**Phosphorous vacancies:** These vacancies are the other common donor in II-IV-P<sub>2</sub> crystals. They are present as singly ionized

donors (V<sub>P</sub><sup>+</sup>) in as-grown crystals and are only converted to neutral donors (V<sub>P</sub><sup>0</sup>) during illuminations at temperatures below 15–20 K. After removing the light, the neutral donors quickly decay at these low temperatures, either by direct transfer of an electron to a nearby acceptor or by the thermal release of an electron from the shallow neutral state to the conduction band. The photoinduced neutral state is paramagnetic but has proven difficult to observe with EPR, primarily because its spectrum is always obscured by the acceptor spectrum that is unavoidably present. There is no resolved hyperfine to aid in identification, and only the anisotropy of the g matrix allows models to be established.

## VII. SUMMARY

Electron paramagnetic resonance (EPR) has been used to identify and characterize native defects in CdGeP<sub>2</sub> crystals. Spectra from cadmium vacancies (V<sub>Cd</sub><sup>-</sup>), germanium-on-cadmium antisites (Ge<sub>Cd</sub><sup>+</sup>), and phosphorous vacancies (V<sub>P</sub><sup>0</sup>) are observed, and their production conditions are described. The analysis of the angular dependence of these EPR spectra gives spin-Hamiltonian parameters and allows models to be established. In the case of the V<sub>Cd</sub><sup>-</sup> acceptor, ENDOR gives additional hyperfine information that is unresolved in the EPR spectra. These ENDOR results verify the significant delocalization of the unpaired spin density around the cadmium vacancy. Broad photoinduced optical absorption bands peaking near 1.05 μm and 756 nm in CdGeP<sub>2</sub> are attributed to native defects. A final section in the paper provides an overview of the dominant donors and acceptors experimentally observed in II-IV-P<sub>2</sub> nonlinear crystals.

## ACKNOWLEDGMENTS

One of the authors (T.D.G.) was supported at the Air Force Institute of Technology by an NRC Research Associateship Award. Any opinions, findings, and conclusions or recommendations expressed in this paper are those of the authors and do not necessarily reflect the views of the United States Air Force.

## AUTHOR DECLARATIONS

### Conflict of Interest

The authors have no conflicts to disclose.

### Author Contributions

**T. D. Gustafson:** Conceptualization (equal); Data curation (equal); Formal analysis (equal); Investigation (equal); Validation (lead); Writing – review & editing (equal). **N. C. Giles:** Conceptualization (equal); Formal analysis (equal); Funding acquisition (equal); Investigation (equal); Resources (equal); Visualization (lead); Writing – review & editing (equal). **P. G. Schunemann:** Conceptualization (equal); Resources (equal); Writing – review & editing (equal). **K. T. Zawilski:** Conceptualization (equal); Resources (equal); Writing – review & editing (equal). **K. L. Averett:** Conceptualization (equal); Funding acquisition (equal); Project administration (equal); Writing – review & editing (equal). **J. E. Slagle:** Conceptualization (equal); Funding acquisition (equal); Project administration (equal); Writing – review & editing

(equal). **L. E. Halliburton:** Conceptualization (equal); Data curation (equal); Formal analysis (equal); Writing – original draft (lead); Writing – review & editing (equal).

## DATA AVAILABILITY

The data that support the findings of this study are available within the article.

## REFERENCES

- <sup>1</sup>J. L. Shay, E. Buehler, and J. H. Wernick, “Electroreflectance, absorption coefficient, and energy-band structure of CdGeP<sub>2</sub> near the direct energy gap,” *Phys. Rev. B* **4**, 2479 (1971).
- <sup>2</sup>G. D. Boyd, E. Buehler, F. G. Storz, and J. H. Wernick, “Linear and nonlinear optical properties of ternary A<sup>II</sup>B<sup>IV</sup>C<sup>V</sup> chalcopyrite semiconductors,” *IEEE J. Quantum Electron.* **QE 8**, 419 (1972).
- <sup>3</sup>J. L. Shay and J. H. Wernick, *Ternary Chalcopyrite Semiconductors: Growth, Electronic Properties, and Applications* (Pergamon Press, New York, 1975).
- <sup>4</sup>V. Petrov, “Frequency down-conversion of solid-state laser sources to the mid-infrared spectral range using non-oxide nonlinear crystals,” *Prog. Quantum Electron.* **42**, 1 (2015).
- <sup>5</sup>P. G. Schunemann, K. T. Zawilski, L. A. Pomeranz, D. J. Creeden, and P. A. Budni, “Advances in nonlinear optical crystals for mid-infrared coherent sources,” *J. Opt. Soc. Am. B* **33**, D36 (2016).
- <sup>6</sup>H. P. Piyathilaka, R. Sooriyagoda, V. Dewasurendra, M. B. Johnson, K. T. Zawilski, P. G. Schunemann, and A. D. Bristow, “Terahertz generation by optical rectification in chalcopyrite crystals ZnGeP<sub>2</sub>, CdGeP<sub>2</sub> and CdSiP<sub>2</sub>,” *Opt. Express* **27**, 16958 (2019).
- <sup>7</sup>V. S. Nozdrin, S. V. Chuchupal, G. A. Komandin, V. N. Kurlov, O. E. Porodinkov, I. E. Spektor, G. M. Katyba, P. G. Schunemann, and K. T. Zawilski, “The influence of defects on the absorption of terahertz radiation in a CdSiP<sub>2</sub> single crystal,” *Opt. Spectrosc.* **128**, 1004 (2020).
- <sup>8</sup>B. N. Carnio, K. T. Zawilski, P. G. Schunemann, O. Moutanabbir, and A. Y. Elezabi, “The coming age of pnictide and chalcogenide ternary crystals in the terahertz frequency regime,” *IEEE Trans. Terahertz Sci. Technol.* **12**, 433 (2022).
- <sup>9</sup>K. Sato, G. A. Medvedkin, T. Nishi, Y. Hasegawa, R. Misawa, K. Hirose, and T. Ishibashi, “Ferromagnetic phenomenon revealed in the chalcopyrite semiconductor CdGeP<sub>2</sub>:Mn,” *J. Appl. Phys.* **89**, 7027 (2001).
- <sup>10</sup>P. Mahadevan and A. Zunger, “Room-temperature ferromagnetism in Mn-doped semiconducting CdGeP<sub>2</sub>,” *Phys. Rev. Lett.* **88**, 047205 (2002).
- <sup>11</sup>K. Sato, G. A. Medvedkin, T. Ishibashi, S. Mitani, K. Takanashi, Y. Ishida, D. D. Sarma, J. Okabayashi, A. Fujimori, T. Kamatani, and H. Akai, “Novel Mn-doped chalcopyrites,” *J. Phys. Chem. Solids* **64**, 1461 (2003).
- <sup>12</sup>V. G. Storchak, D. G. Eshchenko, H. Luetkens, E. Morenzoni, R. L. Lichti, S. F. Marenkin, O. N. Pashkova, and J. H. Brewer, “Room temperature ferromagnetism in III-V and II-IV-V<sub>2</sub> dilute magnetic semiconductors,” *Physica B* **374–375**, 430 (2006).
- <sup>13</sup>M. H. Rakowsky, W. K. Kuhn, W. J. Lauderdale, L. E. Halliburton, G. J. Edwards, M. P. Scripsick, P. G. Schunemann, T. M. Pollak, M. C. Ohmer, and F. K. Hopkins, “Electron paramagnetic resonance study of a native acceptor in as-grown ZnGeP<sub>2</sub>,” *Appl. Phys. Lett.* **64**, 1615 (1994).
- <sup>14</sup>N. C. Giles, L. E. Halliburton, P. G. Schunemann, and T. M. Pollak, “Photoinduced electron paramagnetic resonance of the phosphorus vacancy in ZnGeP<sub>2</sub>,” *Appl. Phys. Lett.* **66**, 1758 (1995).
- <sup>15</sup>L. E. Halliburton, G. J. Edwards, M. P. Scripsick, M. H. Rakowsky, P. G. Schunemann, and T. M. Pollak, “Electron-nuclear double resonance of the zinc vacancy in ZnGeP<sub>2</sub>,” *Appl. Phys. Lett.* **66**, 2670 (1995).
- <sup>16</sup>K. T. Stevens, S. D. Setzler, L. E. Halliburton, N. C. Fernelius, P. G. Schunemann, and T. M. Pollak, “Electron-nuclear double resonance study of the zinc vacancy in zinc germanium phosphide (ZnGeP<sub>2</sub>),” in *Materials Research Society Symposium Proceedings* (MRS Online Proceedings Library, Cambridge University Press, 1998), Vol. 484, p. 549.
- <sup>17</sup>S. D. Setzler, N. C. Giles, L. E. Halliburton, P. G. Schunemann, and T. M. Pollak, “Electron paramagnetic resonance of a cation antisite defect in ZnGeP<sub>2</sub>,” *Appl. Phys. Lett.* **74**, 1218 (1999).
- <sup>18</sup>S. D. Setzler, P. G. Schunemann, T. M. Pollak, M. C. Ohmer, J. T. Goldstein, F. K. Hopkins, K. T. Stevens, L. E. Halliburton, and N. C. Giles, “Characterization of defect-related optical absorption in ZnGeP<sub>2</sub>,” *J. Appl. Phys.* **86**, 6677 (1999).
- <sup>19</sup>W. Gehlhoff, R. N. Pereira, D. Azamat, A. Hoffmann, and N. Dietz, “Energy levels of native defects in zinc germanium diphosphide,” *Physica B* **308–310**, 1015 (2001).
- <sup>20</sup>N. C. Giles, L. Bai, M. M. Chirila, N. Y. Garces, K. T. Stevens, P. G. Schunemann, S. D. Setzler, and T. M. Pollak, “Infrared absorption bands associated with native defects in ZnGeP<sub>2</sub>,” *J. Appl. Phys.* **93**, 8975 (2003).
- <sup>21</sup>W. Gehlhoff, D. Azamat, A. Hoffmann, and N. Dietz, “Structure and energy level of native defects in as-grown and electron-irradiated zinc germanium diphosphide studied by EPR and photo-EPR,” *J. Phys. Chem. Solids* **64**, 1923 (2003).
- <sup>22</sup>W. Gehlhoff, D. Azamat, and A. Hoffmann, “EPR studies of native and impurity-related defects in II-IV-V<sub>2</sub> semiconductors,” *Mater. Sci. Semicond. Process.* **6**, 379 (2003).
- <sup>23</sup>D. M. Hofmann, N. G. Romanov, W. Gehlhoff, D. Pfisterer, B. K. Meyer, D. Azamat, and A. Hoffmann, “Optically detected magnetic resonance experiments on native defects in ZnGeP<sub>2</sub>,” *Physica B* **340–342**, 978 (2003).
- <sup>24</sup>W. Gehlhoff and A. Hoffmann, “EPR identification of intrinsic and transition metal-related defects in ZnGeP<sub>2</sub> and other II-IV-V<sub>2</sub> compounds,” *Physica B* **404**, 4942 (2009).
- <sup>25</sup>G. Medvedkin, “Optical dichroism in ZnGeP<sub>2</sub> crystals at deep levels,” *J. Opt. Soc. Am. B* **39**, 851 (2022).
- <sup>26</sup>W. Gehlhoff, D. Azamat, A. Krtischil, A. Hoffmann, and A. Krost, “EPR and electrical studies of native point defects in ZnSiP<sub>2</sub> semiconductors,” *Physica B* **340–342**, 933 (2003).
- <sup>27</sup>N. C. Giles, L. E. Halliburton, S. Yang, X. Yang, A. T. Brant, N. C. Fernelius, P. G. Schunemann, and K. T. Zawilski, “Optical and EPR study of point defects in CdSiP<sub>2</sub> crystals,” *J. Cryst. Growth* **312**, 1133 (2010).
- <sup>28</sup>E. M. Golden, N. C. Giles, E. Maniego, F. K. Hopkins, K. T. Zawilski, P. G. Schunemann, and L. E. Halliburton, “Identification of native defects (vacancies and antisites) in CdSiP<sub>2</sub> crystals,” *J. Appl. Phys.* **118**, 185702 (2015).
- <sup>29</sup>E. M. Scherrer, B. E. Kananen, E. M. Golden, F. K. Hopkins, K. T. Zawilski, P. G. Schunemann, L. E. Halliburton, and N. C. Giles, “Defect-related optical absorption bands in CdSiP<sub>2</sub> crystals,” *Opt. Mater. Express* **7**, 658 (2017).
- <sup>30</sup>E. M. Scherrer, L. E. Halliburton, E. M. Golden, K. T. Zawilski, P. G. Schunemann, F. K. Hopkins, K. L. Averett, and N. C. Giles, “Electron paramagnetic resonance and optical absorption study of acceptors in CdSiP<sub>2</sub> crystals,” *AIP Adv.* **8**, 095014 (2018).
- <sup>31</sup>P. Zapol, R. Pandey, M. Ohmer, and J. Gale, “Atomistic calculations of defects in ZnGeP<sub>2</sub>,” *J. Appl. Phys.* **79**, 671 (1996).
- <sup>32</sup>X. Jiang, M. S. Miao, and W. R. L. Lambrecht, “Theoretical study of cation-related point defects in ZnGeP<sub>2</sub>,” *Phys. Rev. B* **71**, 205212 (2005).
- <sup>33</sup>X. Jiang, M. S. Miao, and W. R. L. Lambrecht, “Theoretical study of the phosphorus vacancy in ZnGeP<sub>2</sub>,” *Phys. Rev. B* **73**, 193203 (2006).
- <sup>34</sup>X. Jiang and W. R. L. Lambrecht, “The importance of the self-interaction correction for Jahn-Teller distortion of the zinc vacancy in ZnGeP<sub>2</sub>,” *Solid State Commun.* **149**, 685 (2009).
- <sup>35</sup>A. D. Martinez, E. L. Warren, P. Gorai, K. A. Borup, D. Kuciauskas, P. C. Dippo, B. R. Ortiz, R. T. Macaluso, S. D. Nguyen, A. L. Greenaway, S. W. Boettcher, A. G. Norman, V. Stevanović, E. S. Toberer, and A. C. Tamboli, “Solar energy conversion properties and defect physics of ZnSiP<sub>2</sub>,” *Energy Environ. Sci.* **9**, 1031 (2016).
- <sup>36</sup>C. Wang, J. Sun, H. Gou, S. Wang, J. Zhang, and X. Tao, “Intrinsic defects and their effects on the optical properties in the nonlinear optical crystal CdSiP<sub>2</sub>: A first-principles study,” *Phys. Chem. Chem. Phys.* **19**, 9558 (2017).

- <sup>37</sup>M. Huang, S.-S. Wang, Y.-N. Wu, and S. Chen, “Defect physics of ternary semiconductor ZnGeP<sub>2</sub> with a high density of anion cation antisites: A first principles study,” *Phys. Rev. Appl.* **15**, 024035 (2021).
- <sup>38</sup>K. T. Zawilski, P. G. Schunemann, T. M. Pollak, D. E. Zelmon, N. C. Fernelius, and F. Kenneth Hopkins, “Growth and characterization of large CdSiP<sub>2</sub> single crystals,” *J. Cryst. Growth* **312**, 1127 (2010).
- <sup>39</sup>K. Masumoto, S. Isomura, and W. Goto, “The preparation and properties of ZnSiAs<sub>2</sub>, ZnGeP<sub>2</sub>, and CdGeP<sub>2</sub> semiconducting compounds,” *J. Phys. Chem. Solids* **27**, 1939 (1966).
- <sup>40</sup>R. Grigorovici, R. Mănăilă, and A. A. Vaipolin, “The structure of crystalline and amorphous CdGeP<sub>2</sub>,” *Acta Cryst. B* **24**, 535 (1968).
- <sup>41</sup>S. C. Abrahams and J. L. Bernstein, “Luminescent piezoelectric CdSiP<sub>2</sub>: Normal probability plot analysis, crystal structure, and generalized structure of the A<sup>II</sup>B<sup>IV</sup>C<sub>2</sub><sup>V</sup> family,” *J. Chem. Phys.* **55**, 796 (1971).
- <sup>42</sup>M. D. Lind and R. W. Grant, “Structural dependence of birefringence in the chalcopyrite structure.: Refinement of the structural parameters of ZnGeP<sub>2</sub> and ZnSiAs<sub>2</sub>,” *J. Chem. Phys.* **58**, 357 (1973).
- <sup>43</sup>J. A. Van Vechten and J. C. Phillips, “New set of tetrahedral covalent radii,” *Phys. Rev. B* **2**, 2160 (1970).
- <sup>44</sup>G. He, I. Rozahun, Z. Li, J. Zhang, and M.-H. Lee, “Size effect and identified superior functional units enhancing second harmonic generation responses on the II-IV-V<sub>2</sub> type nonlinear optical crystals,” *Chem. Phys.* **518**, 101 (2019).
- <sup>45</sup>S. Stoll and A. Schweiger, “Easyspin, a comprehensive software package for spectral simulation and analysis in EPR,” *J. Magn. Reson.* **178**, 42 (2006).
- <sup>46</sup>See <https://www.easyspin.org> for “The EasySpin program.”
- <sup>47</sup>M. E. Rose, “Chap. IV,” in *Elementary Theory of Angular Momentum* (John Wiley & Sons, New York, 1957), pp. 50–51.
- <sup>48</sup>G. B. Arfken and H. J. Weber, “Chap. 3,” in *Mathematical Methods for Physicists*, 4th ed. (Academic Press, San Diego, CA, 1995), pp. 188–189.
- <sup>49</sup>J.-M. Spaeth and H. Overhof, “Chaps. 5 and 6,” in *Point Defects in Semiconductors and Insulators: Determination of Atomic and Electronic Structure From Paramagnetic Hyperfine Interactions* (Springer-Verlag, Berlin, 2003).
- <sup>50</sup>J. A. Weil and J. R. Bolton, “Chap. 12,” in *Electron Paramagnetic Resonance Elementary Theory and Practical Applications*, 2nd ed. (John Wiley and Sons, Hoboken, NJ, 2007).
- <sup>51</sup>N. J. Stone, “Table of nuclear magnetic dipole and electric quadrupole moments,” *At. Data Nuclear Data Tables* **90**, 75 (2005).
- <sup>52</sup>A. Höglund, C. W. M. Castleton, and S. Mirbt, “Relative concentration and structure of native defects in GaP,” *Phys. Rev. B* **72**, 195213 (2005).
- <sup>53</sup>U. Kaufmann, J. Schneider, and A. Räuber, “ESR detection of antisite lattice defects in GaP, CdSiP<sub>2</sub>, and ZnGeP<sub>2</sub>,” *Appl. Phys. Lett.* **29**, 312 (1976).